AIAA JOURNAL
Vol. 49, No. 1, January 2011

Array Processing for Noisy Data: Application for Open and Closed Wind Tunnels

Daniel Blacodon*
ONERA, 92322 Châtillon, France

DOI: 10.2514/1.J050006

Array processing represents an extremely important area in aeroacoustics: in particular, in the development of methods to extract the useful characteristics of acoustic sources, such as their locations and absolute levels, starting from the received sound field. Generally, the methods are based on a deconvolution operation to remove the undesirable effects of smearing produced by array response. This process should be carried out after the additive noise has been suitably attenuated and, ideally, the deconvolution operator should amplify the noise as little as possible. We show that, when a noise reference is known beforehand, and under certain assumptions, that it is possible to both remove the smearing effect produced by array response and to reduce the noise contamination of the results using a method called the spectral estimation method with additive noise. This method has been applied to computer and experimental simulations involving acoustic sources radiating in a noisy environment. The levels of the sources were found with good accuracy, and the background noise was highly reduced, confirming the validity of the approach and the good performance of the proposed method.

Nomenclature

$\underline{A}(f)$	=	vector of power spectral densities of monopole sources
$A_i(f)$	=	actual power spectral density of ith monopole source
$\hat{A}_i(f)$	=	estimate of $A_i(f)$
$a_i(t)$	=	source function associated to ith monopole source
c	=	speed of sound in propagation medium
$C^{\text{mes}}_{m,n}(\tau)$	=	cross-correlation function between $p^{\text{mes}}_m(t)$ and $p^{\text{mes}}_n(t)$
$C^{\text{mod}}_{m,n}(\tau)$	=	cross-correlation model between $p^{\text{mod}}_m(t)$ and $p^{\text{mod}}_n(t)$
D	=	distance between source region and array
$\mathcal{D}$	=	region containing all acoustic source areas D_q
D_q	=	source area q
$E[.]$	=	expectation operator
f	=	frequency, Hz
$G_{m,i}(f)$	=	$e^{(j2\pi/cf)R_{mi}}/R_{mi}$ is the Green's function for a source point at location i and an observer at location m
i, j	=	indexes of the monopole sources
J	=	number of monopole sources to model in $\mathcal{D}$
j	=	$\sqrt{-1}$
L	=	length of array
M	=	number of microphones of the array
N	=	data samples at sample rate of $1/T$
N_q	=	number of monopole sources in source area q
P_0	=	20 μPa
$p^{\text{mes}}_n(t)$	=	nth microphone measurement signal
$p^{\text{mod}}_n(t)$	=	nth model signal
Q	=	number of source areas in $\mathcal{D}$
R_{in}	=	distance between ith monopole source and nth microphone
S_i	=	name of acoustic source i
T	=	sampling interval, s
t	=	time, s
(x, y)	=	plane containing both the acoustic areas and the array
$[\Gamma^{\text{mes}}(f)]$	=	array cross-spectral matrix computed with noiseless data
$[\hat{\Gamma}^{\text{mes}}(f)]$	=	estimated array cross-spectral matrix computed with noiseless data
$[\Gamma^{\text{mes},N}(f)]$	=	actual array cross-spectral matrix of background noise
$[\hat{\Gamma}^{\text{mes,ref}(N)}(f)]$	=	estimated array cross-spectral matrix of reference noise
$[\hat{\Gamma}^{\text{mes},T}(f)]$	=	$[\hat{\Gamma}^{\text{mes}}(f)] + [\hat{\Gamma}^{\text{mes,ref}(N)}(f)]$, estimated noisy array cross-spectral matrix
$[\Gamma^{\text{mod}}(f)]$	=	model cross-spectral matrix
$\Gamma^{\text{mes}}_{m,n}(f)$	=	cross-spectral density between noiseless signals $p^{\text{mes}}_m(t)$ and $p^{\text{mes}}_n(t)$
$\hat{\Gamma}^{\text{mes}}_{m,n}(f)$	=	estimated cross-spectral density between $p^{\text{mes}}_m(t)$ and $p^{\text{mes}}_n(t)$
$\hat{\Gamma}^{\text{mes,ref}(N)}_{m,n}(f)$	=	estimated cross-spectral density between noise signals measured with microphones m and n
$\hat{\Gamma}^{\text{mes},T}_{m,n}(f)$	=	estimated cross-spectral density of the noisy signals measured with microphones m and n
$\Gamma^{\text{mod}}_{m,n}(f)$	=	cross-spectral density between $p^{\text{mod}}_m(t)$ and $p^{\text{mod}}_n(t)$ microphones m and n
Δ_s	=	minimum distance between two monopole sources
δ_{ij}	=	Kronecker delta
$\sigma^2_B(f)$	=	variance of white background noise at frequency f
τ	=	time delay
Ω_q	=	power spectral density of acoustic source q

Presented as Paper 2009-3125 at the 15th AIAA/CEAS Aeroacoustics Conference/30th AIAA Aeroacoustics Conference, Miami, FL, 11 May–13 June 2009; received 17 June 2009; revision received 6 April 2010; accepted for publication 12 July 2010. Copyright © 2010 by ONERA. Published by the American Institute of Aeronautics and Astronautics, Inc., with permission. Copies of this paper may be made for personal or internal use, on condition that the copier pay the $10.00 per-copy fee to the Copyright Clearance Center, Inc., 222 Rosewood Drive, Danvers, MA 01923; include the code 0001-1452/11 and $10.00 in correspondence with the CCC.

*Research Engineer, Computational Fluid Dynamics and Aeroacoustics Department, BP72; Daniel.Blacodon@onera.fr.

I. Introduction

A PHASED microphone array is currently used in acoustic tests run in wind tunnels to localize and rank the acoustic sources based on a model of uncorrelated monopole sources [1–6]. It has been successfully applied in the characterization of airframe noise of an aircraft model [7–10]. Other methods considered [11–13] are based on a model of correlated monopole sources to assess the directivity of sources.

However, the performance of the imaging processing may be affected by background noise that usually makes the results

unreliable. This situation arises, for example, in wind tunnels with a closed test section where acoustic sources radiate in a very noisy environment, which makes it difficult to characterize them.

The problem becomes critical when corrupting noise is changing the actual levels and the spectral distribution in the measured cross-spectral matrix (CSM). Besides, undesired dominant noise sources may be present in the corrupting noise, making it more difficult to decide in the localization maps whether the sources with high levels correspond to those of interest or not.

To get over this drawback, a lot of research on the modeling and removal of the effects of noise and distortion has been done. The main conclusions of these studies are that the success of noise-processing methods depends on their ability to characterize and model the noise process and to use the noise characteristics advantageously to differentiate the signal from the noise. Various techniques such as beamforming (nonadaptive and adaptive) and spatial-temporal filtering can be used to achieve noise reduction [14–17]. In certain applications, it is not possible to access the instantaneous frame of the contaminating noise, and only the noisy signal is available. Thus, the noise cannot be cancelled out, but it may be reduced, in an average sense, using the statistics of the signal and the noise process. In other situations, it is not possible to get a noise reference: the reference signal can either be generated artificially or extracted from the primary signal or from the imaging results [18].

Sometimes we have access to a noise reference and, under some assumptions on the noise characteristics, it is possible to use several strategies to remove its effects. An interesting approach proposed in [19] shows how the generalized singular value decomposition can be used to achieve noise reduction. Another popular solution uses the spectral subtraction method to reduce the noise contamination [20]. It is based on the subtraction of the short-term spectral magnitude of noise from that of the noisy spectrum. A generalized form of the basic spectral subtraction is given in [21], where power spectral subtraction uses short-time power spectrum estimates instead of a magnitude spectrum.

The present study is focused on the presentation of an extension of the spectral estimation method (SEM) [4], which is based on a prior knowledge of a noise [22]. This new method called SEM with additive noise (SEMWAN) has the advantage of being able to reduce the smearing effect due to the array response and, at the same time, the inaccuracy of the results caused by noise sources, which can be coherent as well as incoherent, with high or low levels. This method is well suited to applications in a wind tunnel since we can, for example, get a noise reference or record the environmental noise before installing the models in the test section.

This paper is organized as follows. Section II begins with a presentation of the problem estimation of the actual levels of acoustic sources, starting from noiseless data with the SEM. The assessment of the performance of the SEM in the estimation of the acoustic source levels starting from noisy data is also examined. Section III is devoted to the presentation of methods aiming to reduce the noise pollution in the results. In particular, it describes the power spectrum subtraction (PSS), which is very simple to implement, and the principle of SEMWAN. SEM and SEMWAN are applied on numerical simulations and experimental simulations in Secs. IV and V, respectively. Results of tests carried out in open and closed wind tunnels are presented in Sec. VI.

II. Least-Squares Solution for Source Level Estimation from Noiseless Data

We consider the geometry depicted in Fig. 1, where an overall source domain located in the (x, y) plane split into Q (with $Q = 2$) effective noise radiating areas S_q (the subscript $q = 1, 2$) in a noiseless environment. An array of M microphones located in front of $\mathcal{D}$ records the radiated pressure. We assume that the acoustic sources are random and stationary.

The objective here is to find the location of S_1 and S_2 and estimate Ω_1 and Ω_2, their absolute levels starting from the acoustic signals provided by the microphones of the array.

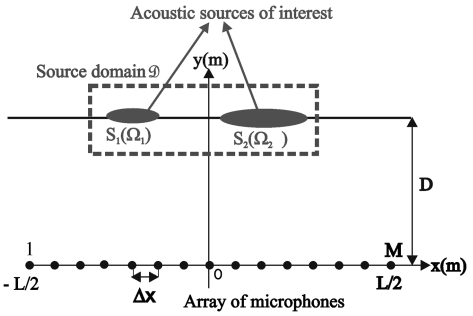

Fig. 1 Geometry of the problem of acoustic SPL estimation using noiseless data.

A. Array and Model Cross-Spectral Matrix

The characterization of the acoustic sources in location and level is based on the CSM $[\Gamma^{\text{mes}}(f)]$ computed with the output signals and on $[\Gamma^{\text{mod}}(f)]$, a modeling of this matrix.

1. *Array Cross-Spectral Matrix*

Let $p_n^{\text{mes}}(t)$ be the pressure recorded by the microphone n. The cross-correlation function $C_{m,n}^{\text{mes}}(\tau)$ between the microphone signals n and m is defined as

$$C_{m,n}^{\text{mes}}(\tau) = E[p_m^{\text{mes}}(t)p_n^{\text{mes}}(t+\tau)] \tag{1}$$

The cross-power spectral $\Gamma_{m,n}^{\text{mes}}(f)$ between $p_m^{\text{mes}}(t)$ and $p_n^{\text{mes}}(t)$ is the Fourier transform of $C_{m,n}^{\text{mes}}(\tau)$ (Wiener–Khintchine theorem):

$$\Gamma_{m,n}^{\text{mes}}(f) = \int_{-\infty}^{\infty} C_{m,n}^{\text{mes}}(\tau)e^{2\pi jf\tau}\,\mathrm{d}\tau \tag{2}$$

The measured array CSM of all signals $p_m^{\text{mes}}(t)$ $(m = 1, 2, \ldots, M)$ is defined by

$$[\hat{\Gamma}^{\text{mes}}(f)] = \begin{bmatrix} \hat{\Gamma}_{1,1}^{\text{mes}}(f) & . & \hat{\Gamma}_{1,M}^{\text{mes}}(f) \\ . & . & . \\ \hat{\Gamma}_{M,1}^{\text{mes}}(f) & . & \hat{\Gamma}_{M,M}^{\text{mes}}(f) \end{bmatrix}$$

2. *Model Cross-Spectral Matrix*

The array CSM can be viewed as a direct measurement of the source power levels of interest. Since the array CSM is known, the problem here is to find the parameters (i.e., the power levels of the source areas) of a model matrix with respect to the observed CSM. A standard approach in the estimation procedure consists of sampling the source areas D_q $(q = 1, \ldots, Q)$ and considering that, at each sampling point so obtained, there are candidate sources for which the powers remain to be found.

In the paper, one considers that the acoustic source areas D_q $(q = 1, \ldots, Q)$ are each modeled with a set of N_q closely spaced (with respect to the acoustic wavelength) uncorrelated monopoles. It follows that the total number of virtual sources used to characterize all the source areas is $J = \sum_{q=1}^{Q} N_q$.

It is pointed out here that a distribution of monopoles, dipoles, or quadrupoles is suitable to achieve the modeling of the source areas. However, the choice to use monopole source distributions is not based on any assumption about the structure of the actual sources. It has been chosen because this is the simplest equivalent model. Furthermore, a monopole source distribution does not mean that the directivity pattern is a priori isotropic: correlated monopoles with phase relationships can model any directivity pattern [11]. So, a valuable equivalent source model could be a set of correlated monopoles. It is clear that the problem of finding both the amplitude of the sources and their correlation function in amplitude and phase involves a very large number of parameters. It is difficult to solve this problem at this level using a limited number of microphones. Fortunately, a majority of noise sources of interest in our experiments have smooth directivity patterns. This means that if the aperture angle of an array of microphones seen from the overall source region is not

too large, the directivity pattern of each region may be considered as isotropic within this aperture.

Let us consider that each monopole is characterized with a source function $a_i(t)$. The correlation function between the ith and jth monopoles is

$$C_{i,j}(\tau) = E[a_i(t)a_j(t+\tau)] = C_i(\tau)\delta_{i,j} \tag{3}$$

The spectrum of $a_i(t)$ is $A_i(f)$: the Fourier transform of $C_i(\tau)$ [Eq. (3)]. The problem of the source level estimation is then to find the J parameters $A_i(f)$ of the model for each frequency. To proceed, it is necessary to define the general structure of the array CSM for uncorrelated monopole sources and then choose the J parameters $A_i(f)$ such that the model CSM is a best fit to the measured spectral power levels (SPLs).

To compute the model CSM, we begin by expressing the radiated pressure on the array:

$$p_n(t) = \sum_{i=1}^{J} \frac{a_i(t - R_{in}/c)}{R_{in}} \tag{4}$$

where R_{in} is the distance from the source i to the microphone n. The model cross-correlation function $C^{\text{mod}}_{m,n}(\tau)$ between the microphone signals n and m is defined as

$$C^{\text{mod}}_{m,n}(\tau) = E[p^{\text{mod}}_m(t)\, p^{\text{mod}}_n(t+\tau)] \tag{5}$$

One obtains from Eqs. (4) and (5) for $C^{\text{mod}}_{m,n}(\tau)$,

$$C^{\text{mod}}_{m,n}(\tau) = \sum_{i=1}^{J} \frac{C_i[\tau + (R_{im} - R_{in})/c]}{R_{im}R_{in}} \tag{6}$$

The Fourier transform of $C^{\text{mod}}_{m,n}(\tau)$ gives the model for the CSM:

$$\Gamma^{\text{mod}}_{m,n}(f) = \sum_{i=1}^{J} \frac{e^{jk(R_{im}-R_{in})}}{R_{im}R_{in}} A_i(f) \tag{7}$$

For the further developments, $\Gamma^{\text{mod}}_{m,n}(f)$ is written with the following compact form:

$$\Gamma^{\text{mod}}_{m,n}(f) = \sum_{i=1}^{J} G_{m,i}(f)A_i(f)G^*_{n,i}(f) \tag{8}$$

B. Theoretical Background of Spectral Estimation Method

Consider $[\Gamma^{\text{mes}}(f)]$, the array CSM, and $[\Gamma^{\text{mod}}(f)]$, the model CSM due to the acoustic sources of component $\Gamma^{\text{mod}}_{m,n}(f)$. In SEM [4], the problem of finding the power spectral densities (PSDs) $A_i(f)$ is based on the following cost function:

$$E[\underline{A}(f)] = \sum_{m,n=1}^{M} \left| \hat{\Gamma}^{\text{mes}}_{m,n}(f) - \sum_{j=1}^{J} G_{m,j}(f)A_j(f)G^*_{n,j}(f) \right|^2 \tag{9}$$

The minimization of the mean-squares error $E[\underline{A}(f)]$ between the array and model matrices with respect to $\underline{A}(f)$ leads to the square linear system:

$$\sum_{j=1}^{J} V_{i,j}(f)A_j(f) = U^S_i(f) \tag{10}$$

with

$$U^S_i(f) = \sum_{m,n=1}^{M} G_{m,i}(f)\hat{\Gamma}^{\text{mes}}_{m,n}(f)G^*_{m,i}(f)$$

$$V_{i,j}(f) = \left| \sum_{m=1}^{N} G_{m,i}(f)G^*_{m,j}(f) \right|^2$$

The resolution of Eq. (10) provides the estimates $\hat{A}_i(f)$ of the desired PSDs $A_i(f)$. However, solutions $A_i(f)$, obtained after the minimization process, are not guaranteed to be positive. This can lead to physically unrealistic solutions for the recovered spectra (i.e., spectra with negative amplitudes). Adding a positivity constraint on parameters $A_i(f)$ can easily circumvent this drawback. This can be done using a new set of parameters, such as $\alpha^2_j(f) = A_i(f)$, which implicitly contain the constraint of positivity. After this step, one obtains a problem without constraint of the following form:

$$F[\underline{\alpha}(f)] = \sum_{m,n=1}^{M} \left| \Gamma^{\text{mes}}_{m,n}(f) - \sum_{j=1}^{J} G_{m,j}(f)\alpha^2_j(f)G^*_{n,j}(f) \right|^2 \tag{11}$$

Now two questions arise: on the existence of a unique global minimum (uniqueness of the solution) and on the choice of the initial guess to find a global minimum (and not a local one).

It is generally difficult to answer these questions theoretically when the estimation problem has nonlinearity characteristics, such as the one that is under study in the paper. Today, we may only say that we have obtained different solutions and minima starting from very different values of the initial guess. However, it has been found in all the simulations performed that the initial guess $\alpha^2_i(f) = U_i(f)$ leads to the global minimum, although we lack general proof for this observation.

1. *Source Power Levels Estimation with Spectral Estimation Method*

The computation procedure consists of first sampling the source areas and then determining the power levels $\hat{\alpha}^2_j(f)$ of virtual uncorrelated monopoles located at each of the sampling points by minimizing the error in Eq. (11).

Among all the methods available to perform nonlinear optimization [23], we chose an efficient and robust algorithm called the restarted conjugate gradient method to compute the $\hat{\alpha}^2_j(f)$. This method is well documented from a statistical point of view [24] and from a numerical point of view [25]. An efficient well-debugged software version of the algorithm is available [26]. The minimization of the cost function $F[\underline{\alpha}(f)]$ with respect to $\alpha_j(f)$ provides positive noise-free PSDs, as will be shown in the next section. After this step, the total power level output $\Omega_q(f)$ of the source area D_q is obtained by summing the power levels $\hat{\alpha}^2_j(f)$ of all monopole sources that are used in the modeling of D_q:

$$\Omega_q(f) = \sum_{j=1}^{N_q} \hat{\alpha}^2_j(f) \tag{12}$$

The SEM is the overall technique aimed at finding $\Omega_q(f)$.

The result is valid only around the direction $\mathbf{u}$ and in the aperture $\Delta\mathbf{u}$ of the measuring array, seen from the source region. Consequently, in the acoustic far field, the SPL at a large distance R from the sources and around the direction $\mathbf{u}$ is modeled as

$$P(f, R\mathbf{u}) = \sum_{q=1}^{Q} \frac{\Omega_q(f)}{R^2} \tag{13}$$

$\Omega_q(f)$ may be considered as the mean directivity pattern of each radiating area q in the direction $\mathbf{u}$ averaged on $\Delta\mathbf{u}$. Then, rotating the measuring array around the global radiating region enables us to estimate the full directivity pattern.

2. *Limitation of Spectral Estimation Method when Using Noisy Data*

The SEM described previously gives reliable results when it is applied to noiseless data or when the signal-to-noise ratio is high. However, in many practical situations, the development of a new aircraft is often based on experiments conducted in a closed wind tunnel. In these cases, the acoustic measurements are carried out with wall-mounted arrays, which are contaminated by noise emanating from fans, support masts, and by flow noise. It is thus necessary to examine the ability of SEM to characterize the acoustic sources radiating in a noisy environment. This study is based on the same situation shown in Fig. 1, but this time, the wave fields radiated by S_1 and S_2 are the corrupted coherent noise S_3 (i.e., fan noise) of PSD

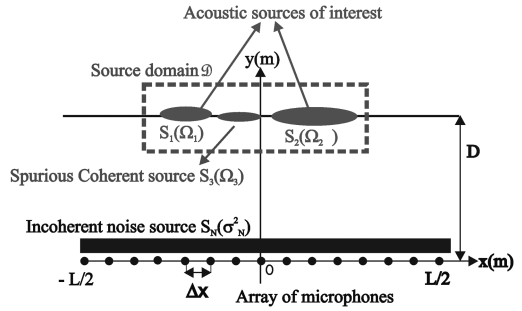

Fig. 2 Geometry of the problem of acoustic SPL estimation using noisy data.

$\Omega_3(f)$ and an incoherent broadband noise S_N (i.e., flow noise) of variance $\sigma_B^2(f)$ (Fig. 2).

It is assumed that the source and the noise signals are uncorrelated. It follows that a realistic noisy array cross-power spectral $[\hat{\Gamma}^{\text{mes},T}(f)]$ can be expressed as the sum of $[\hat{\Gamma}^{\text{mes}}(f)]$ and $[\hat{\Gamma}^{\text{mes},N}(f)]$, which are the cross-power spectral matrices of the acoustic sources and of the overall noise sources, respectively, so that we have

$$[\hat{\Gamma}^{\text{mes},T}(f)] = [\hat{\Gamma}^{\text{mes}}(f)] + [\hat{\Gamma}^{\text{mes},N}(f)] \tag{14}$$

The accuracy of the $\hat{A}_i(f)$ depends on the variance of the background noise. Indeed, consider that the acoustic sources radiate in an ideal medium without background noise or, equivalently, when the noise CSM $[\hat{\Gamma}^{\text{mes},N}(f)]$ is null. $[\hat{\Gamma}^{\text{mes}}(f)]$ may be assumed as equal to $[\Gamma^S(f)]$, the source CSM that would be obtained with noiseless data. The estimates $\hat{A}_i(f)$ obtained by solving Eq. (10) will allow characterizing of the actual levels of the acoustic sources, as was shown with numerical simulations presented in [4].

In contrast, when the propagation medium is corrupted with background noise, the minimization cost function for obtaining the parameters $\hat{A}_i(f)$ is based on this relation:

$$\sum_{j=1}^{J} V_{i,j}(f) S_j(f) = U_i^S(f) + U_i^N(f) \tag{15}$$

Equation (15) may be written with the following compact form as

$$\sum_{j=1}^{J} V_{i,j}(f) A_j(f) = U_i^N(f)\left[1 + \frac{U_i^S(f)}{U_i^N(f)}\right] \tag{16}$$

We may analyze Eq. (16) as follows:

1) When the power ratio verifies $[U_i^S(f)]/U_i^N(f)][\gg 1$, the estimated parameters will allow an estimation of the acoustic source levels with a high degree of accuracy.

2) When the power ratio verifies $[U_i^S(f)]/[U_i^N(f)] \ll 1$, the estimated parameters $\hat{A}_i(f)$ will characterize the undesired background noise.

3) In the other situations, actual PSDs of the acoustic source will be more or less corrupted by background noise.

III. Noise Reduction Methods

The conclusion drawn in the previous section is that the SEM will give results that are strongly erroneous if applied to very noisy data. It was shown that the lower the magnitude of the background noise, the more accurate the estimates of the source PSDs. It is obvious that a reduction of the noise will generally improve the accuracy of array processing methods. In the continuation of the section, one considers two approaches to reduce the spurious effects on the results provided by SEM. They are both based on measurement of a noise reference, which are assumed to correctly characterize the noise sources.

A. Power Spectrum Subtraction

A very simple way to achieve this, when a noise reference is available, consists of subtracting the noise reference from the noisy spectra. However, while this solution is very attractive because the computational complexity of the spectral subtraction is not expensive, it has a major drawback. The effectiveness of the noise removal process is dependent on obtaining an accurate spectral estimate of the noise signal. The better the noise estimate, the lower the level of residual noise appearing in the modified spectrum. However, since the noise spectrum cannot be directly obtained, it is necessary to use an averaged estimate of the noise. Hence, there are some significant variations between the estimated noise spectrum and the actual noise content present in the instantaneous spectra corrupted by the background noise. The subtraction of these quantities results in the presence of isolated residual noise levels of large variance. The increase in the variance constitutes an irrevocable distortion in the reconstructed spectra.

B. Least-Squares Solution for Source Level Estimation with Noisy Data

The conclusion drawn in Sec. II is that the SEM will give results that are strongly erroneous if applied to very noisy data. This drawback may be removed with the SEMWAN, which is an improvement of SEM. This implies taking into account the contribution of the background noise in the acoustic measurements and modifying the optimization problem using Eqs. (11) and (14) so that we obtain

$$F[\underline{A}(f)] = \sum_{m,n=1}^{M} \left| \hat{\Gamma}_{m,n}^{\text{mes},T}(f) - \hat{\Gamma}_{m,n}^{\text{mes},N}(f) - \sum_{j=1}^{J} G_{m,j}(f) A_j(f) G_{n,j}^*(f) \right|^2 \tag{17}$$

The cross-power spectral matrix $[\hat{\Gamma}^{\text{mes},N}(f)]$ is generally not available, because the measurements of acoustic sources and of noise sources cannot be obtained separately. A way to overcome this difficulty consists of modeling the noise sources, as was done for the acoustic sources in Eqs. (7) and (8). The problem is not so simple, because noise sources are many and varied in wind tunnels and include wind, vibrations, and fan. Furthermore, most noise signals of interest are at least partly random. Hence, it is not possible to formulate an equation that can predict the exact future values of random signals, because they have unpredictable fluctuations. Therefore, without any a priori information about the noise, it is very difficult (or even impossible) to solve the estimation problem defined by Eq. (17). However, the characteristics of the noise can be easily measured in the absence of the model. The received signals during this measurement are obviously made up only of noises. Indeed, the antenna collects the whole of the unwanted noise. It is interesting to consider that the noise is stationary and that its observation duration is infinite, which makes it possible to deduce its CSM $[\hat{\Gamma}^{\text{mes,ref}(N)}(f)]$. These assumptions are tractable, because the noise sources in the turbulent boundary layer flowing over the microphones in the wind tunnel are stationary. The same remark can be applied to the noise radiated by the fan, the support mast, or for all the parasitic noise sources generated in the wind tunnel.

At this point of the paper, one considers several assumptions about the noise reference sources and the acoustic sources:

1) The magnitude of the noise reference measured before the tests without the acoustic sources is equal to its level produced during the tests with the acoustic sources.

2) The source signals and additive noise components are statistically independent.

It follows from the previous assumptions that $[\hat{\Gamma}^{\text{mes,ref}(N)}(f)]$ can be considered as a very good characterization of $[\hat{\Gamma}^{\text{mes},N}(f)]$, so that it is possible to replace $[\hat{\Gamma}^{\text{mes},N}(f)]$ with $[\hat{\Gamma}^{\text{mes,ref}(N)}(f)]$ in Eq. (18):

$$F[\underline{A}(f)] = \sum_{m,n=1}^{M} \left| \hat{\Gamma}_{m,n}^{\text{mes},T}(f) - \hat{\Gamma}_{m,n}^{\text{mes,ref}(N)}(f) - \sum_{j=1}^{J} G_{m,j}(f) A_j(f) G_{n,j}^{*}(f) \right|^2 \quad (18)$$

Let us develop Eq. (17) in the following form:

$$F[\underline{A}(f)] = C^{\text{mes}}(f) - 2\sum_{j=1}^{J} U_j^{\text{mes}}(f) A_j(f) + 2\sum_{j=1}^{J} U_j^{N}(f) S_j(f) + C^{N}(f) - 2C^{\text{mes},N}(f) + \sum_{i,j}^{J} A_i(f) V_{i,j}(f) A_j(f) \quad (19)$$

with

$$C^{\text{mes}}(f) = \sum_{m=1}^{M}\sum_{n=1}^{M} |\Gamma_{m,n}^{\text{mes},T}(f)|^2$$

$$U_i^{\text{mes}}(f) = \sum_{m=1}^{M}\sum_{n=1}^{M} G_{m,i}(f) \Gamma_{m,n}^{\text{mes},T}(f) G_{n,i}^{*}(f)$$

$$U_i^{N}(f) = \sum_{m=1}^{M}\sum_{n=1}^{M} G_{m,i}(f) \Gamma_{m,n}^{\text{mes,ref}(N)}(f) G_{n,i}^{*}(f)$$

$$C^{N}(f) = \sum_{m=1}^{M}\sum_{n=1}^{M} |\Gamma_{m,n}^{\text{mes},ref(N)}(f)|^2$$

$$C^{\text{mes},N}(f) = \sum_{m=1}^{N}\sum_{n=1}^{N} \Gamma_{m,n}^{\text{mes},T*}(f) \Gamma_{m,n}^{\text{mes},ref(N)}(f)$$

and

$$V_{i,j}(f) = \left| \sum_{m=1}^{M} G_{m,i}(f) G_{m,j}^{*}(f) \right|^2$$

The noise-free PSDs $A_i(f)$ are defined as the solution of the following problem:

$$\hat{A} = \arg\min_{A} F(\underline{A}) \quad (20)$$

As for the SEM, to ensure positivity of the spectra, a new set of parameters is introduced, such as $\beta_j^2(f) = A_i(f)$. Thus, the least-squares problem can be formulated as follows:

$$H[\underline{\beta}(f)] = C^{\text{mes}} - 2\sum_{j=1}^{J} U_j^{\text{mes}}(f) \beta_j^2(f) + 2\sum_{j=1}^{J} U_j^{N}(f) \beta_j^2(f) + C^{N}(f) - 2C^{\text{mes},N}(f) + \sum_{i,j}^{J} \beta_i^2(f) V_{i,j}(f) \beta_j^2(f) \quad (21)$$

In this form, it appears that the cost function $H[\underline{\beta}(f)]$ takes into account 1) the bias due to the variance of the background noise with $C^N(f)$, 2) the background noise that was propagated in the source domain with $U_i^N(f)$, and 3) the background that may be correlated with the acoustic sources with $C^{\text{mes},N}(f)$.

The computation procedure developed for the SEMWAN is quite similar to the one presented for SEM in Sec. II.B.1. The minimization of the cost function $H[\underline{\beta}(f)]$ with respect to $\alpha_j(f)$ provides positive noise-free PSDs. The total power level output $\Omega_q(f)$ of the source area D_q is obtained by summing the power levels $\hat{\beta}_j^2(f)$ of all monopole sources that are used in the modeling of D_q:

$$\tilde{\Omega}_q(f) = \sum_{j=1}^{N_q} \hat{\beta}_j^2(f) \quad (22)$$

We will call SEMWAN this overall technique aimed at finding $\tilde{\Omega}_q(f)$.

IV. Numerical Simulations

The purpose of this section is to evaluate the ability of SEMWAN to accurately estimate the levels and locations of two extended acoustic sources, S_1 and S_2, radiating at a frequency of $f = 4$ kHz in a noisy environment (Fig. 2). S_1 and S_2 are composed of 40 uncorrelated monopoles evenly spaced with $\Delta_s = 0.005$ m. The levels of each monopole source for S_1 and S_2 are $20\log[A_1(f)] = 55$ dB and $20\log[A_2(f)] = 70$ dB, respectively. The integrated power level for S_1 is given by the following relation:

$$\Omega_1(f) = 10\log\sum_{j=1}^{40} A_j^2(f) = 71.02 \text{ dB} \quad (23)$$

If we substitute A_1 by A_2 in Eq. (23), we find that the integrated power level for S_2 is equal to $\Omega_2(f) = 86.02$ dB.

The wave fields generated by the two sources are assumed to be measured by a linear array of length $L = 1.4$ m, with $M = 15$ microphones separated by 0.1 m (Fig. 2). The distance between the array and the source line is $D = 2$ m.

To simulate the noisy environment, the virtual microphone signals are contaminated: on the one hand with an additive coherent noise source S_3 composed of 24 uncorrelated monopole sources, each with a level of $20\log[A_3(f)] = 50$ dB, such that the integrated power levels $\Omega_3(f) = 63.8$ dB, and on the other hand, with an incoherent noise S_4 with a variance in decibels equal to $(\sigma_B^2)_{\text{dB}} = 60$ dB (Fig. 3).

A. Results with Conventional Beamforming, Spectral Estimation Method, and Spectral Estimation Method with Additive Noise for $(\sigma_B^2)_{\text{dB}} = 60$ dB

Figure 4 shows the result given by conventional beamforming (CBF) and the SEM at the emission frequency of 4 kHz for the configuration presented in Fig. 3. Predictably, CBF neither resolves the two extended sources S_1 and S_2 nor gives their actual levels. In contrast, SEM separates S_1 and S_2 and correctly characterizes the two sources in both location and levels. It also appears that the coherent spurious source S_3 is found with SEM. However, it will be difficult to decide in practical situations if S_3 is a source of interest or not. We also observe several unwanted sources due to the incoherent background noise.

Figure 5 shows the noise reference (i.e., S_3 and S_N) used to compute $[\hat{\Gamma}^{\text{mes,ref}(N)}(f)]$ and, in Fig. 6, the result provided by SEMWAN. Now, the spurious sources are removed, and S_1 and S_2 are found at their actual locations with their levels within 1 dB.

B. Results with Spectral Estimation Method and Spectral Estimation Method with Additive Noise for $[\sigma_B^2(f)]_{\text{dB}} = 80$ dB

We consider, in Fig. 7, a configuration with a high level of 80 dB for S_N. This situation may be representative of the tests carried out in a wind tunnel with a closed test section. The characteristics of the acoustic sources S_1 and S_2 and of the spurious source S_3 remain unchanged compared with those presented in Fig. 3.

The degradation of the result found by the SEM (Fig. 8) is clear compared with that shown in Fig. 4. It is not possible to distinguish

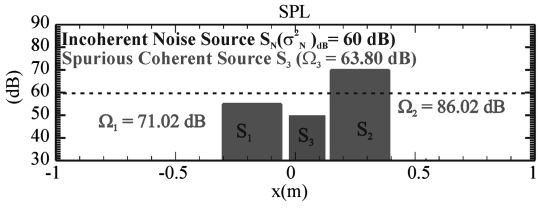

Fig. 3 Simulation of two extended sources, S_1 and S_2, contaminated by a coherent noise source S_3 and a broadband noise with a variance of 60 dB.

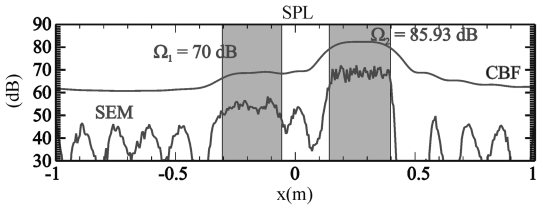

Fig. 4 Result obtained with CBF and SEM for the configuration presented in Fig. 3.

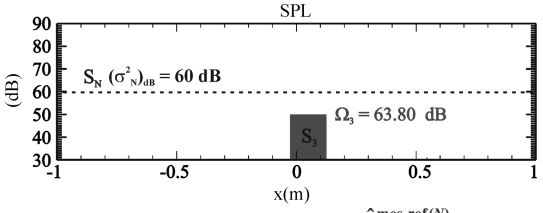

Fig. 5 Noise references used to compute $[\hat{\Gamma}^{mes,ref(N)}(f)]$ and apply SEMWAN for the configuration presented in Fig. 3.

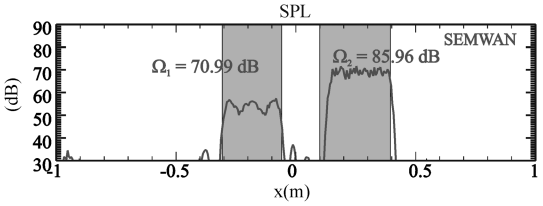

Fig. 6 Result obtained with SEMWAN using noise references presented in Fig. 5 for configuration.

the sources S_1 and S_2, because the result is completely erratic over the whole computational domain. This is in agreement with the study described in Sec. II. Figure 9 shows the noise reference used by SEMWAN, and Fig. 10 shows the result obtained with this method. Now, S_1 and S_2 are resolved, their levels are correctly estimated, and the smearing effect of the background noise is removed.

In many applications, one may want to characterize only one or several desired noise sources with particular features but discard the rest of the uninteresting sources and noises. This is, for example, the case when we are interested in assessing noise produced by an innovative device installed on a model without having the corruption

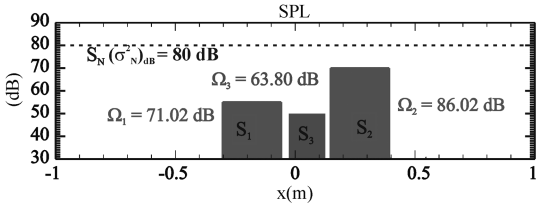

Fig. 7 Simulation of two extended sources, S_1 and S_2, contaminated by a coherent noise source S_3 and a broadband noise with a variance of 80 dB.

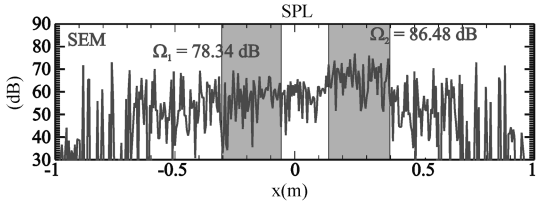

Fig. 8 Result obtained with SEM for the configuration presented in Fig. 7.

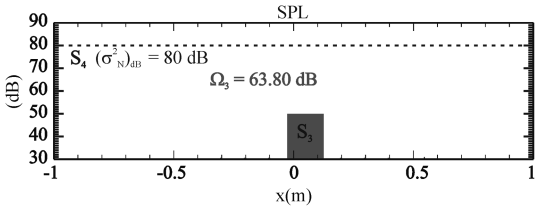

Fig. 9 Noise references used to construct $[\hat{\Gamma}^{mes,ref(N)}(f)]$ and apply SEMWAN for the configuration presented in Fig. 7.

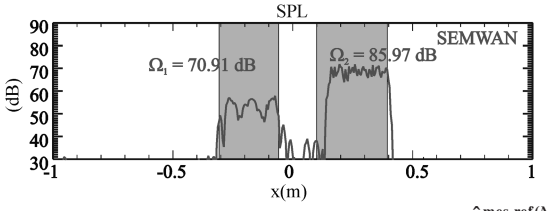

Fig. 10 Result obtained with SEMWAN using $[\hat{\Gamma}^{mes,ref(N)}(f)]$ computed with the noise references given in Fig. 9 for the configuration shown in Fig. 7.

from other noise sources. In this particular situation, a noise reference measured when the device is removed from the model will allow SEMWAN to reduce the levels of the sources produced by the model due to the background noise but leave the levels of sources generated by the device unchanged. This situation is considered in Fig. 6, where the device of interest is characterized by the source S_3, and the noise reference is defined by S_1, S_2, and S_N (Fig. 11). The result presented in Fig. 12 shows that the undesired noise sources are removed with SEMWAN and that S_3 is correctly characterized in location and level.

V. Experimental Simulations

A simple experiment was conducted in an anechoic chamber to validate SEMWAN with experimental data. A picture and a schematic view of the experimental setup are presented in Figs. 13 and 14, respectively. We consider here that the acoustic sources are three driver units, S_1, S_2, and S_3, mounted in the middle of a wooden plate and spatially separated at 0.29 m. The background noise is generated by the driver units S_4 and S_5 placed near the array of microphones and between the two wooden plates separated by 3 m. The phased array is composed of 30 microphones ($\frac{1}{2}$ in. 3211 Brüel and Kjaer) evenly spaced at 10 cm.

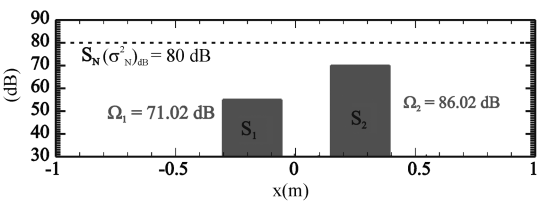

Fig. 11 Noise references used to apply SEMWAN for the configuration presented in Fig. 7.

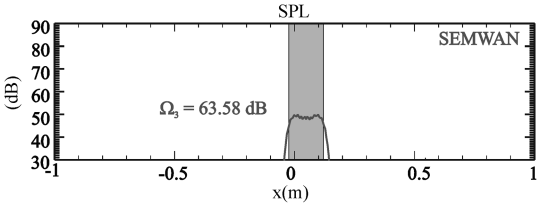

Fig. 12 Result obtained with SEMWAN using noise references given in Fig. 11 for configuration shown in Fig. 7.

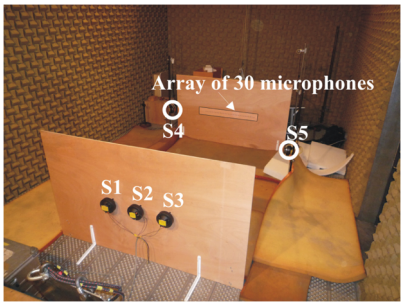

Fig. 13 Experimental setup used to validate SEMWAN.

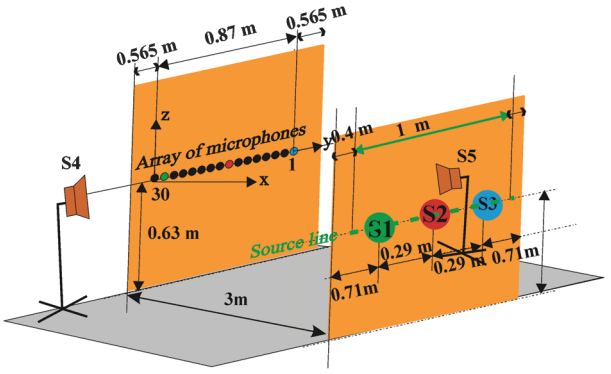

Fig. 14 Schematic view of the experimental setup in the anechoic chamber.

A. Methodology of the Tests

The driver units S_1, S_2, and S_3 were connected independently to three generators delivering sinusoidal signals at the frequency of 2.5, 4.83, and 8 kHz, respectively. The driver units S_4 and S_5 were also connected at independent generators delivering a broadband signal filtered at 10 kHz for S_4 and a sinusoidal signal at 3 kHz for S_5. The acoustic waves radiated by each of the five driver units were individually measured by the array of microphones. The spectra of S_1, S_2, S_3, S_4, and S_5 are presented in Figs. 15 and 16. The levels of the spectra measured by microphones 29, 15, and 1 opposite the sources S_1, S_2, and S_3, respectively, will be compared with the results provided by the SEM and SEMWAN. Thus, it will possible to assess the ability of both methods to accurately reproduce the levels of acoustic sources radiating in a noisy environment. The noise reference matrix $[\hat{\Gamma}^{\text{mes,ref}(N)}(f)]$ required by SEMWAN is computed with the data measured when only S_4 and S_5 impinge on the array of microphones. An example of the spectra of $[\hat{\Gamma}^{\text{mes,ref}(N)}(f)]$ is presented in Fig. 17. It shows the broadband noise and emerging tone noise of about 10 dB at 3 kHz.

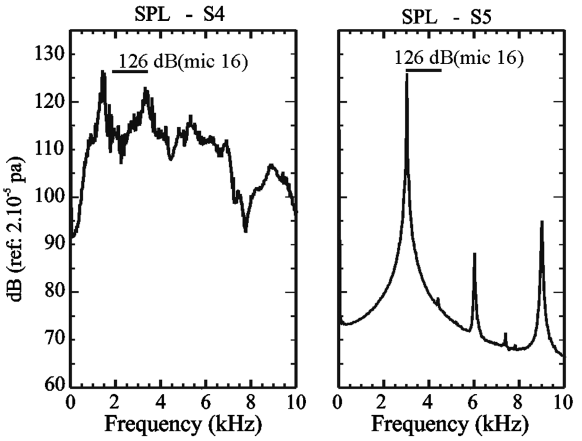

Fig. 16 Spectra of the noise sources S_4 and S_5.

B. Data Processing

The array cross-power matrices $[\hat{\Gamma}^{\text{mes},T}(f)]$ and $[\hat{\Gamma}^{\text{mes,ref}(N)}(f)]$ were estimated using 200 data blocks, of 1024 samples each, sampled at 31,250 Hz (i.e., $\Delta f = 31,250/1024 = 30.51$ Hz). The levels of $N_q = 200$ virtual monopole sources were computed at spatial sampling points equally spaced every $\Delta y = 0.005$ m, on a line passing through the middle of the driver units S_1, S_2, and S_3, from $y = 0.4$ m up to $y = 1.4$ m, at the discrete frequencies $f_g = g\Delta f$ ($g = 1, \ldots, 328$) and in the frequency range [0, 10 kHz]. The measured spectra are compared with the estimated spectra with the SEM and SEMWAN after their propagation at the location of microphone n using, respectively, the following relations:

$$P_n^{\text{SEM}}(f) = 10\log\left[\left(\sum_{j=1}^{N_q}\frac{\hat{\alpha}_j^2(f)}{R_{nj}^2}\right)/P_0^2\right] \tag{24}$$

$$P_n^{\text{SEMWAN}}(f) = 10\log\left[\left(\sum_{j=1}^{N_q}\frac{\hat{\beta}_j^2(f)}{R_{nj}^2}\right)/P_0^2\right] \tag{25}$$

C. Results

Presented in this section is a result obtained with PSS, compared with the performance of the SEM and SEMWAN: first in the characterization of the sources S_1 and S_2, then S_2 and S_3 when the array measurements are contaminated by S_4 and S_5.

1. *Performance of Power Spectrum Subtraction*

The left side of Fig. 18 presents the spectra of S_1 and S_2 (black curve) and the spectrum $\hat{\Gamma}_{16,16}^{\text{mes},T}(f)$ of the signal of microphone 16 when S_1, S_2, S_4, and S_5 impinge on the array. Superimposed on the right side of Fig. 18 is the spectrum of microphone 16 (black curve)

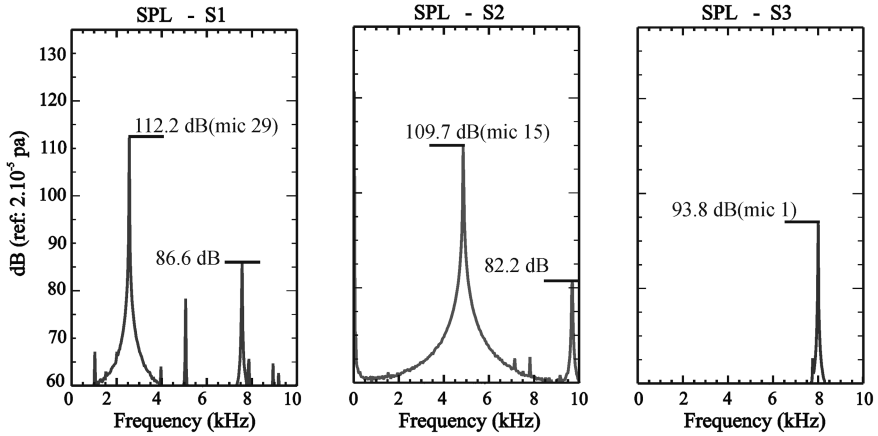

Fig. 15 Spectra of the acoustic sources S_1, S_2, and S_3.

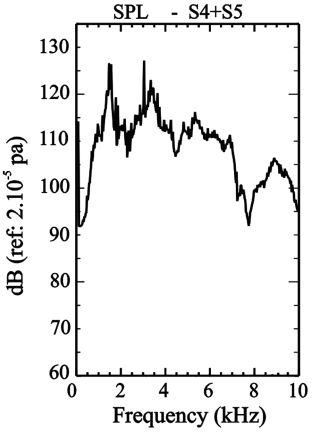

Fig. 17 Measured spectrum with microphone 16 when S_4 and S_5 impinge on the array of microphones.

and the result found with PSS (gray curve) obtained by subtracting the spectrum $\hat{\Gamma}_{16,16}^{\text{mes,ref}(N)}(f)$ of the noise-reference measured with microphone 16 from $\hat{\Gamma}_{16,16}^{\text{mes},T}(f)$.

Reduction of the background is obtained with PSS, but there are a lot of frequency components with negative levels, certainly due to the weak signal-to-noise ratio considered in this test. We can also see that the sources S_1 and S_2 do not clearly appear at their emission frequencies. This result is a good illustration of the drawbacks of PSS.

2. Performance of Spectral Estimation Method and Spectral Estimation Method with Additive Noise

Considered here is the same configuration as in the previous section. Figure 19 shows the result given by the SEM [Eq. (24)]. The level of the fundamental component of S_1 is found with a great accuracy, while that of S_2 is underestimated by about 3 dB. There are also numerous spurious sources with high levels generated by S_4 and S_5.

The result given by SEMWAN [Eq. (25)] is presented in Fig. 20. The noise sources have been highly reduced, as well as the levels of the fundamental components of S_1 and S_2 and the second harmonic of S_1 found within 1 dB. This demonstrates how SEMWAN can reduce the undesired noises and sources when a noise reference is available.

The second scenario is shown in the graph on the left side of Fig. 21, where the characterization of S_2 and S_3 is considered, with the two sources corrupted by S_4 and S_5. The graph on the right side of Fig. 21 shows the result with the SEM. The levels of the fundamental component of S_2 are underestimated by about 3 dB, while those of S_3 are within 1.5 dB. Again, there are numerous spurious sources with high levels due to S_4 and S_5.

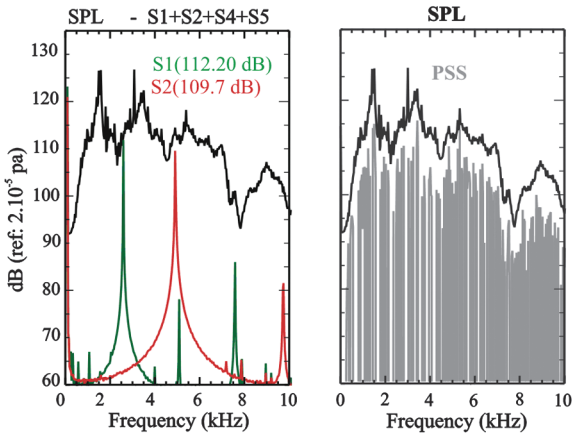

Fig. 18 Result obtained with the PSS method for the spectrum of microphone 16 with the spectrum shown in Fig. 17 used as noise reference.

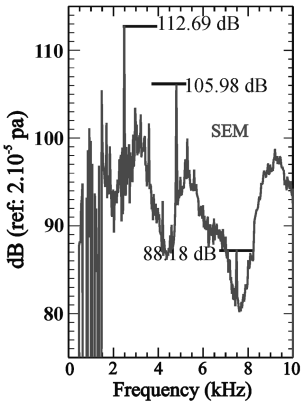

Fig. 19 Result found with SEM for the configuration shown on the left side of Fig. 18.

The result obtained with SEMWAN (see Fig. 22) shows that S_2 and S_3 appear more clearly due to the reduction of noise. The level of the fundamental component of S_1 is accurately estimated and that of S_2 is obtained within 2.54 dB. However, it is difficult to observe the first harmonic of S_2, which is embedded in the background noise. It also appears that S_1 has not been completely removed by SEMWAN.

VI. Experimental Results

The SEM and SEMWAN were applied to data recorded during three test campaigns. The first was conducted in the ONERA Centre d'Essais des Propulseurs (CEPRA) 19 wind tunnel with a 1:11th scale A320/A321. The objective here was to use SEMWAN to extract the noise radiated by the landing gear.

The second and third tests took place in the closed and open test sections of the large low-speed facility (LLF) German–Dutch wind tunnels (DNW), respectively, with a 1:0.6th scale A340 Airbus model. The SEMWAN was used to remove the background noise contaminating measurements taken in the closed test section of the DNW, thus obtaining absolute levels for the acoustic sources radiated by the model. The results obtained with the SEM and SEMWAN in the closed test section were compared with the measured spectra in the open test section of the LLF–DNW.

A. Tests Carried out in the Centre d'Essais des Propulseurs 19 ONERA Wind Tunnel

A 1:11th scale A320/A321 Airbus model was tested in the CEPRA 19 anechoic wind tunnel by ONERA, as part of the European project for the reduction of airframe and installation noise and under a contract from Airbus Industries and SPAé (French Aeronautic Programs Service) [7,27]. The objective of this experiment was to identify and quantify the contribution of airframe noise sources to the overall acoustic noise radiated in the far field.

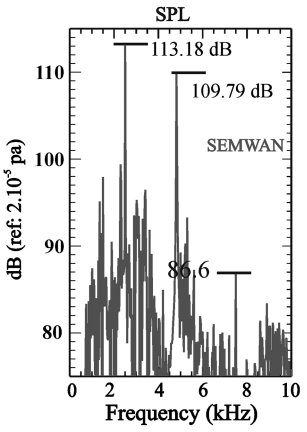

Fig. 20 Result found with SEMWAN for the configuration presented on the left side of Fig. 18.

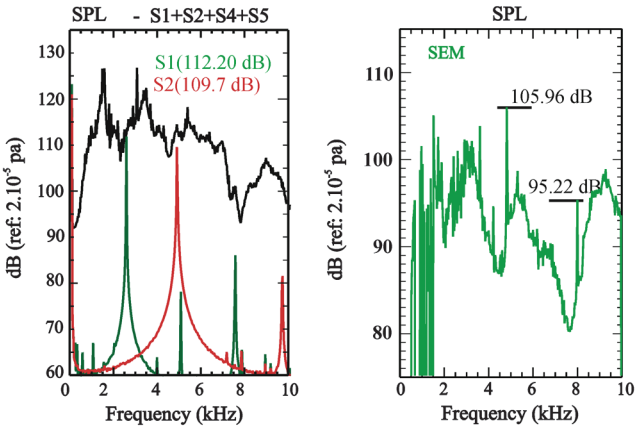

Fig. 21 Spectra of acoustic sources S_2 and S_3 to estimate and the spectrum measured by microphone 16 due to S_2, S_3, S_4,and S_5 (left). Result found with SEM (right).

1. Experimental Setup in Centre d'Essais des Propulseurs 19 and Data Processing

The experimental setups with and without the landing gear are presented in Fig. 23. The test considered here was carried out with the deflection angle of the slats fixed at 27°, the flaps deployed with an angle of 25°, the angle of attack set at 6°, and a flow velocity of 60 m/s. The phased array is composed of two crossed subarrays with 40 $\frac{1}{2}$ in. microphones (AKSUD 3211). It was positioned out of the flow at a distance of 2.4 m from the longitudinal axis of the aircraft model. Consequently, the correction of refraction and the convection effects of the acoustic rays between the focus points on the aircraft model and the microphones of the array were taken into account [28,29] in the model CSM to obtain actual locations and levels of the acoustic sources.

The array cross-spectral matrices $[\hat{\Gamma}^{\text{mes},T}(f)]$ and $[\hat{\Gamma}^{\text{mes,ref}(N)}(f)]$ measured, respectively, when the gear, deployed and retracted, was estimated using 200 data blocks, including 1024 samples, each at the sampling frequency f_s. All the SPLs were computed up to $f_{\max} = f_s/2$. They are plotted versus normalized frequencies f/f max in the range [0, 1]. The sampling grid used by the SEM and SEMWAN to compute the output levels of the complete wing is shown in Fig. 24.

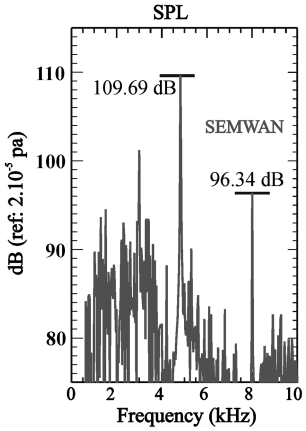

Fig. 22 Result with SEMWAN for the configuration presented on the left in Fig. 21.

The overall measured spectrum with microphone 18 at the center of the array (see Fig. 22) up to the frequency $f_{\max} = f_s/2$ is compared with the integrated power levels of the 10 source regions (Fig. 25) S_q $(q = 1, 2, \ldots, 10)$, computed with the SEM and SEMWAN and using Eqs. (24) and (25), respectively.

2. Results

The spectra estimated with the SEM are shown in Fig. 26 (green curve) for the 10 subregions when the nose and main landing gears were deployed. The contribution of each of the 10 subregions can be compared with the spectrum of microphone 18 (see Fig. 22) superimposed in Fig. 26. The airframe sources generated by the landing gear are not dominant. Indeed, noise on the slats predominates on its outboard part, at the junction between the slats and the nacelle.

SEMWAN is applied to the test, using as a noise reference the CSM $[\hat{\Gamma}^{\text{mes,ref}(N)}(f)]$ computed when the landing gear is retracted. Clearly, the levels of the source areas that do not contribute to the noise generated by the landing gear are reduced, as shown in Fig. 26 (purple curve).

In the last result presented in Fig. 27, the integrated spectra obtained with the SEM (green curve) and SEMWAN (purple curve) for the complete wing are compared with the measured spectrum (red curve). The result provided by the SEM is very close to the spectrum measured with microphone 18 (see Fig. 22). In contrast, the integrated power level obtained with SEMWAN is about 10 dB lower, because it characterizes only the noise radiated by the landing gear.

B. Tests Carried out in the Closed and Open Test Sections of the Large Low-Speed Facility German–Dutch Wind Tunnels

Within the framework of the European aircraft wing with advanced technology operation project, a test campaign was performed with a 1:10.6-scaled Airbus A340-300 model to assess both the aerodynamic and acoustic properties of different wing devices. For this purpose, two series of tests took place in the LLF–DNW wind tunnel.

1. Experimental Setup in Large Low-Speed Facility German–Dutch Wind Tunnels and Data Processing

The first series of tests were carried out in a LLF–DNW closed test section to assess the aerodynamic properties of the new wing elements. In parallel, acoustic wall array measurements were done to check that innovative devices did not generate excess aerodynamic noise. The test setup, including the model and the three acoustic wall arrays in the floor of the test section, are presented in Fig. 28. The three microphone arrays consisted of LinearX M51 $\frac{1}{2}$ in. microphones, and they were flush mounted in the tunnel floor below the right wing of the model. The use of three arrays allowed detection of noise radiation in forward, downward, and rearward directions. However, the results presented in this section were obtained with the

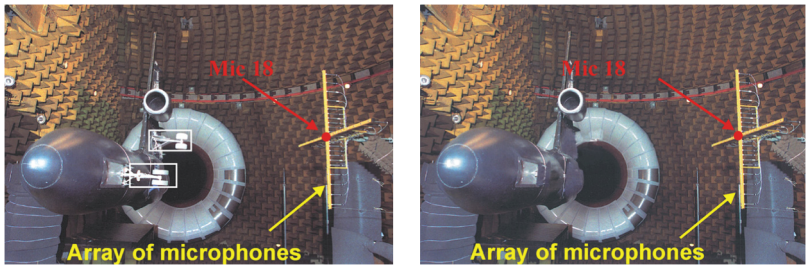

Fig. 23 Detailed view of the test setup in CEPRA 9 with the A320/A321 aircraft model when the landing gear is set and removed.

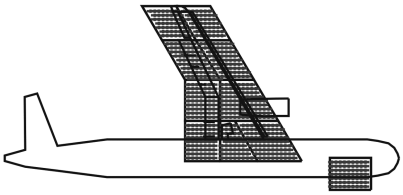

Fig. 24 Computational grid uses by SEM and SEMWAN.

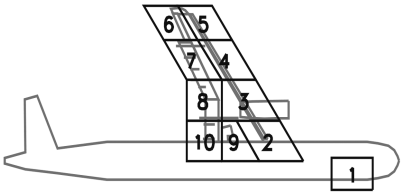

Fig. 25 Ten source areas considered in the study of airframe noise of the 1:11th scale A320/A321 Airbus.

central array, which is sensitive to the dominant acoustic sources radiated on the ground by the model.

The second series of tests was carried out in a LLF–DNW open test section to assess the levels of the acoustic sources radiated by the new wing elements. The test setup, including the model and the array of microphones, are presented in Fig. 29. The microphone array is composed of 143 LinearX M51 $\frac{1}{2}$ in. microphones mounted out of flow below the left wing.

During the experiments in the open and closed test sections, the data measured with the arrays of microphones were digitized and processed with the acquisition and computation systems implemented in the LLF–DNW wind tunnel. Then, with these data, a CSM was computed for each test point. The different steps to obtain the cross-spectral matrices are not given in this section, but they are detailed in [30]. We would like to point out here that the correction of refraction and convection effects of the acoustic rays between the focus points on the aircraft model and the microphones of the array are taken into account in the model CSM [22,23]. In contrast, only the correction of convection effects is considered in the model CSM, when the data are measured in the closed test section.

The sampling grid used by the SEM and SEMWAN to compute the output levels of both wings is presented in Fig. 30. The array matrix

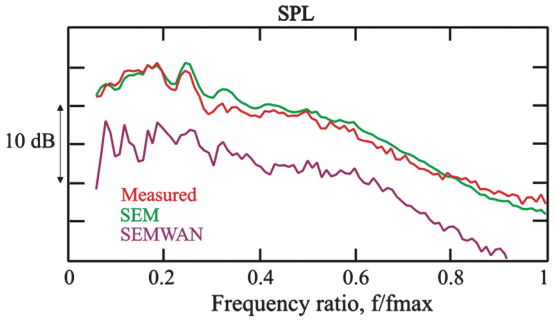

Fig. 27 Comparison between the estimated spectra with SEM and SEMWAN for the complete wing and measured with microphone 18 (see Fig. 22) of the array.

Fig. 28 Test setup in DNW closed test section, with three wall arrays installed on the floor.

$[\hat{\Gamma}^{\text{mes},T}(f)]$ needed by the SEM and SEMWAN was measured in the closed and open test sections during a landing configuration with an angle of attack of 6° and a flow velocity of 60 m/s. The geometrical angles of attack were slightly lower in the closed section and slightly higher in the open jet, in order to compensate for the open jet effect and obtain the same lift. The noise reference matrix $[\hat{\Gamma}^{\text{mes,ref}(N)}(f)]$ was measured in the closed test section during a clean configuration. The overall measured spectrum with microphone 53 (see Fig. 29) of the phased array installed in the open test section, in the frequency range [0, 30 kHz], is compared with the integrated power levels due to both wings being computed with the SEM and SEMWAN.

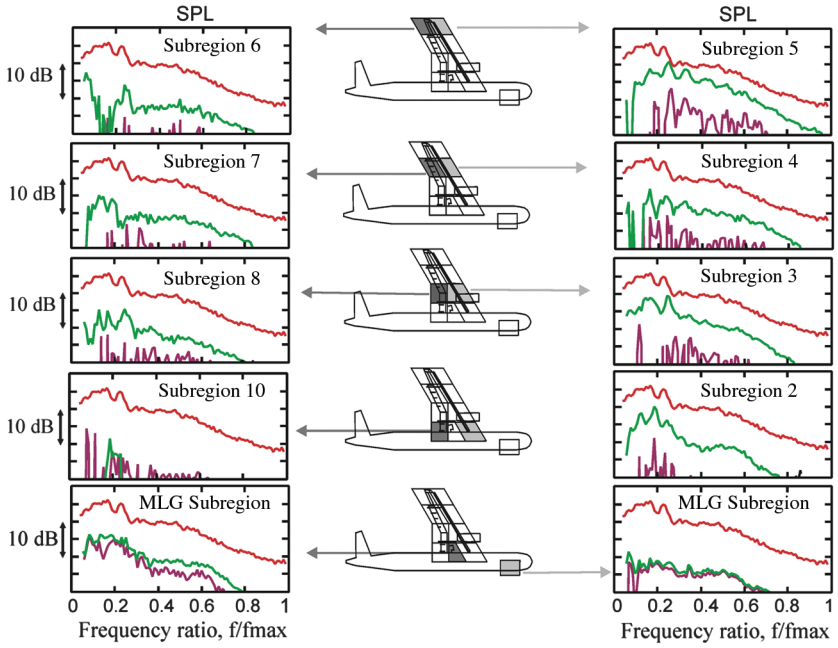

Fig. 26 Spectra computed with SEM (green curve), spectra computed with SEMWAN (purple curve), and measured spectrum (red curve) (MLG denotes main landing gears, and NLG denotes nose landing gear).

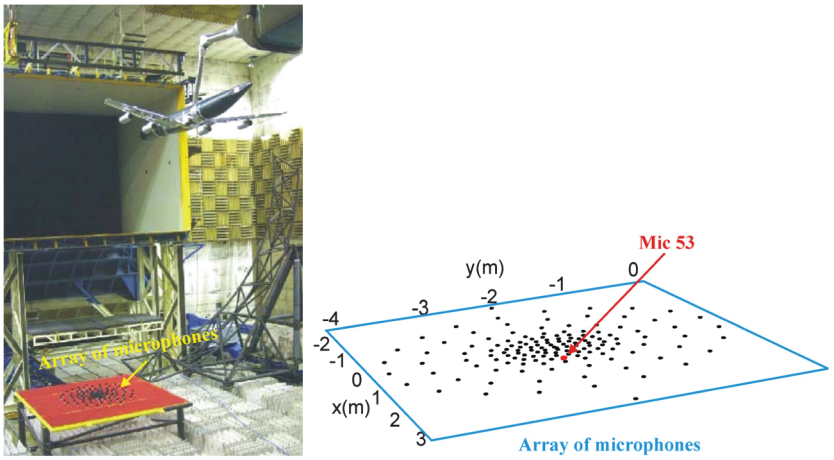

Fig. 29 Test setup in DNW open jet. The out-of-flow microphone array is shown in black.

2. Results

The integrated spectrum estimated with the SEM for both wings starting from the signals measured in the open test section of the LLF–DNW wind tunnel is compared in Fig. 31 with the spectrum measured in the open test section with microphone 53 (see Fig. 29) of the phased array. There is a very good agreement between the measured spectrum (red curve) and the estimated spectrum (green curve) in the whole frequency band considered here. However, although the SEM is able to successfully estimate the measured spectrum with a single microphone up to 30 kHz, it provides correct results only at low frequencies where coherence loss effects are small in the shear layer of the open jet wind tunnel. Indeed, since these effects are neither taken into account in the source model nor corrected in the array CSM, the SEM and the measured spectra underestimate the source levels at high frequencies.

Figure 32 compares the results obtained with the SEM and SEMWAN starting from measured signals in the closed test section and the measured spectrum with microphone 53 (see Fig. 29) of the phased array installed in the open test section. There is a good agreement between the estimated spectrum with SEMWAN (green curve) and the measured spectrum (red curve) below 10 kHz. The discrepancy above 10 kHz is certainly due to the fact that the levels of measured spectrum are corrupted by the coherence loss effects of the open jet wind tunnel at high frequencies, but not the levels of the estimated spectrum, since these effects do exist in the closed section of the wind tunnel.

The spectrum estimated with the SEM (blue curve) starting from the measured signal in the closed test section is superimposed in Fig. 32. As could be expected, there is an overestimation of the source levels in the whole of the frequency band, because the high tunnel background noise levels have not been taken into account in the SEM.

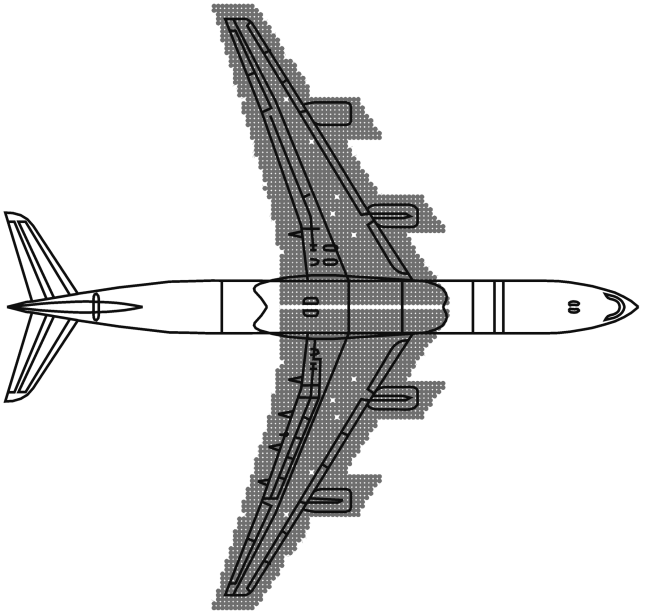

Fig. 30 Spatial sampling of both wings used by SEM and SEMWAN.

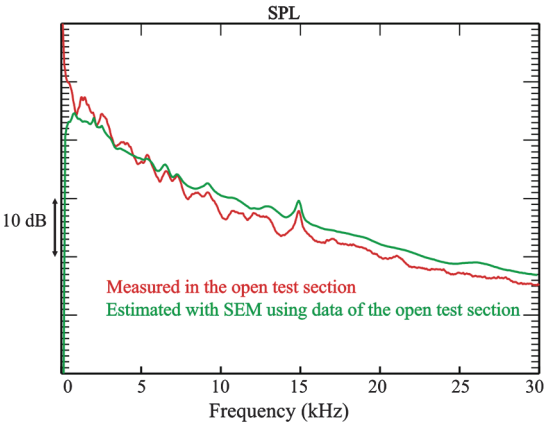

Fig. 31 Comparison of the estimated spectra with SEM and SEMWAN for the complete wing and measured with microphone 53 (see Fig. 29).

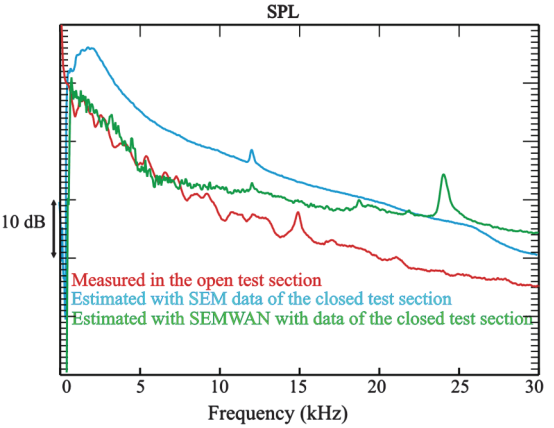

Fig. 32 Comparison of the estimated spectra with SEM and SEMWAN for the complete wing and that measured with the microphone 53 (see Fig. 29).

VII. Conclusions

This study has presented a new method to estimate the actual levels of acoustic sources radiated in a noisy environment. This method called SEMWAN is based on the prior knowledge of a noise reference. Minimizing of the cost function constructed with the noise reference, the array and model matrices, gives solutions with a highly reduced background noise and source levels with good accuracy. SEMWAN has been applied to computer and experimental simulations to estimate the levels of acoustic sources radiated in a noisy environment. The results have confirmed the validity of the approach and the performance of the proposed method.

Acknowledgments

This work was supported by the Department of Numerical Simulation and Aeroacoustics at ONERA. The author is grateful to M. M. Williams Denis and Fabrice Desmerger for many stimulating discussions. The experiment with aircraft model A320 was performed under a contract from Airbus Industries and SPAé (French Service of Aeronautic Programs). The tests with the aircraft model A340 were defined and managed by DLR, Airbus, and the German–Dutch wind tunnels as part of the European advanced wing with advanced technology operation project sponsored by the European Commission.

References

[1] Élias, G., "Source Localization with a Two-Dimensional Focused Array- Optimal Processing for a Cross-Shaped Array," *Inter-Noise 95*, Newport Beach, CA, Noise Control Foundation, New York, 10–12 July 1995, pp. 1175–1178

[2] Élias, G., and Malarmey, C., "Utilisation d'Antennes Focalisées pour la Localisation de Sources Acoustiques," *Revue d'Acoustique*, Vol. 6, Presses Univ. de France, Paris, 1983, pp. 163–166.

[3] Brooks, T., "A Deconvolution Approach for the Mapping of Acoustic Sources (DAMAS) Determined from Phased Microphone Arrays," 10th AIAA/CEAS Aeroacoustics Conference, Manchester, U. K., AIAA Paper 2004-2954, 10–12 May 2004.

[4] Blacodon, D., and Elias, G., "Level Estimation of Extended Acoustic Sources Using a Parametric Method," *Journal of Aircraft*, Vol. 41, No. 6, 2004, pp. 1360–1369. doi:10.2514/1.3053

[5] Sijtsma, P., "CLEAN Based on Spatial Source Coherence," 13th AIAA/CEAS Aeroacoustics Conference, Rome, AIAA Paper 2007-3436, 21–23 May 2007.

[6] Humphreys, W. M., Brooks, T. F., Hunter, W. W., and Meadows, K. R., "Design and Use of Microphone Directional Arrays for Aeroacoustic Measurements," 36th Aerospace Sciences Meeting and Exhibit, Reno, NV, AIAA Paper 1998-0471, 12–15 Jan. 1998.

[7] Blacodon, D., "Analysis of the Airframe Noise of an A320/A321 with a Parametric Method," *Journal of Aircraft*, Vol. 44, No. 1, 2007, pp. 26–34. doi:10.2514/1.20295

[8] Piet, J. F., and Élias, G., "Airframe Noise Source Localization Using a Microphone Array," AIAA/CEAS Aeroacoustics Conference, Atlanta, GA, AIAA Paper 1997-1643, May 1997.

[9] Davy, D., and Remy, H., "Airframe Noise Characteristics of a 1/11 Model Airbus," 4th AIAA/CEAS Aeroacoustics Conference, Toulouse, France, AIAA Paper 1998- 2335, 2–4 June 1998.

[10] Davy, R., Moens, F., and Rémy, H., "Aeroacoustic Behavior of a 1/11 Scale Airbus Model in the Open Anechoic Wind Tunnel CEPRA 19," 8th AIAA/CEAS Aeroacoustics Conference and Exhibit, Breckenridge, CO, AIAA Paper 2002-2412, 17–19 June 2002.

[11] Fleury, V., "Determination of Acoustic Directivity from Microphone Array Measurements Using Correlated Monopoles," 14th AIAA/CEAS Aeroacoustics Conference, Vancouver, AIAA Paper 2008-2855, 5–7 May 2008.

[12] Brooks, T., "Extension of DAMAS Phased Array Processing for Spatial Coherence Determination (DAMAS-C)," 12th AIAA/CEAS Aeroacoustics, Cambridge, MA, AIAA Paper 2006-2654, 8–10 May 2006.

[13] Miles, J., "Procedure for Separating Noise Sources In Measurements of Turbofan Engine Core Noise," 12th AIAA/CEAS Aeroacoustics Conference, Cambridge, MA, AIAA Paper 2006- 2580, 8–10 May 2006.

[14] Doclo, S., and Moonen, M., "Gsvd-Based Optimal Filtering for Single and Multimicrophone Speech Enhancement," *IEEE Transactions on Signal Processing*, Vol. 50, No. 9, 2002, pp. 2230–2244. doi:10.1109/TSP.2002.801937

[15] Cox, H., Zeskind, R. M., and Owen, M. M., "Robust Adaptive Beamforming," *IEEE Transactions on Acoustics, Speech, and Signal Processing*, Vol. 35, No. 10, 1987, pp. 1365–1375. doi:10.1109/TASSP.1987.1165054

[16] Capon, J., "High Resolution Frequency-Wavenumber Spectrum Analysis," *Proceedings of the IEEE*, Vol. 57, No. 8, 1969, pp. 1408–1418. doi:10.1109/PROC.1969.7278

[17] Frost, O. L., "An Algorithm for Linearly Constrained Adaptive Array Processing," *Proceedings of the IEEE*, Vol. 60, No. 8, 1972, pp. 926–935. doi:10.1109/PROC.1972.8817

[18] Koop, L., "Microphone-Array Processing for Wind-Tunnel Measurements with Strong Background Noise," 14th AIAA/CEAS Aeroacoustics Conference, Vancouver, AIAA Paper 2008-2907, 5–7 May 2008.

[19] Bulté, J., "Acoustic Array Measurements in Aerodynamic Wind Tunnels : A Subspace Approach for Noise Suppression," 13th AIAA/CEAS Aeroacoustics Conference, Rome, AIAA Paper 2007-3446, 21–23 May 2007.

[20] Boll, S. F., "Suppression of Acoustic Noise in Speech Using Spectral Subtraction," *IEEE Transactions on Acoustics, Speech, and Signal Processing*, Vol. 27, No. 2, 1979, pp. 113–120. doi:10.1109/TASSP.1979.1163209

[21] Berouti, M., Schwartz, R., and Makhoul, J., "Enhancement of Speech Corrupted by Acoustic Noise," *Proceedings of the IEEE International Conference on Acoustics, Speech, and Signa1 Processing*, IEEE Publ., Piscataway, NJ, April 1979, pp. 208–211.

[22] Comon, P., and Lacoume, J. L., "Noise Reduction for an Estimated Wiener Filter Using Noise References," *IEEE Transactions on Information Theory*, Vol. 32, No. 2, 1986, pp. 310–313. doi:10.1109/TIT.1986.1057146

[23] Gill, P. E., Muttey, W., and Wright, M. H., *Practical Optimization*, Academic Press, London, 1981, pp. 59–66.

[24] Bard, Y., *Nonlinear Parameter Estimation*, Academic Press, New York, 1974.

[25] Bandler, J. W., "Computed-Aided Circuit Optimization," *Modern Filter Theory and Design*, edited by G. C. Temes, and Mitra, S. K., Wiley, New York, 1973.

[26] Shanno, D. F., and Phua, K. H., "Remark on 'Algorithm 500: Minimization of Unconstrained Multivariate Functions [E4]'," *ACM Transactions on Mathematical Software*, Vol. 6, No. 4, 1980, pp. 618–622. doi:10.1145/355921.355933

[27] Davy, R., Moens, F., and Rémy, H., "Aeroacoustic Behavior of a 1/11 Scale Airbus Model in the Open Anechoic Wind Tunnel CEPRA 19," AIAA Paper 2002-2412, June 2002.

[28] Candel, S., Guédel, A., and Julienne, A., "Radiation, Refraction and Scattering on Waves in a Shear Flow," AIAA Paper 1976-544, July 1976.

[29] Amiet, R. K., "Refraction of Sound by a Shear Layer," *Journal of Sound and Vibration*, Vol. 58, No. 4, 1978, pp. 467–482. doi:10.1016/0022-460X(78)90353-X

[30] Oerlemans, S., Broersma, L., and Sijtsma, P., "Quantification of Airframe Noise Using Microphone Arrays in Open and Closed Wind Tunnels," *International Journal of Aeroacoustics*, Vol. 6, No. 4, 2007, pp. 309–333. doi:10.1260/147547207783359440

M. Glauser
Associate Editor